THE UNIVERSITY of EDINBURGH

Edinburgh Research Explorer

Glioblastoma stem cells induce quiescence in surrounding neural stem cells via Notch signalling.

Citation for published version:
Lawlor, K, Marques, MA, Dharmalingham, G, El-Azhar, Y, Schneider, MD, Pollard, SM & Rodriguez, TA 2020, 'Glioblastoma stem cells induce quiescence in surrounding neural stem cells via Notch signalling.', *Genes and Development*. https://doi.org/10.1101/gad.336917.120

Digital Object Identifier (DOI):
10.1101/gad.336917.120

Link:
Link to publication record in Edinburgh Research Explorer

Document Version:
Peer reviewed version

Published In:
Genes and Development

General rights
Copyright for the publications made accessible via the Edinburgh Research Explorer is retained by the author(s) and / or other copyright owners and it is a condition of accessing these publications that users recognise and abide by the legal requirements associated with these rights.

Take down policy
The University of Edinburgh has made every reasonable effort to ensure that Edinburgh Research Explorer content complies with UK legislation. If you believe that the public display of this file breaches copyright please contact openaccess@ed.ac.uk providing details, and we will remove access to the work immediately and investigate your claim.

Download date: 04. Jan. 2021

Glioblastoma stem cells induce quiescence in surrounding neural stem cells via Notch signalling.

Katerina Lawlor[1], Maria Angeles Marques-Torrejon[2], Gopuraja Dharmalingham[3], Yasmine El-Azhar[1], Michael D. Schneider[1], Steven M. Pollard[2§] and Tristan A. Rodríguez[1§]

[1]National Heart and Lung Institute, Imperial College London, Hammersmith Hospital Campus, Du Cane Road, London W12 0NN, UK.

[2]Centre for Regenerative Medicine & Edinburgh Cancer Research UK Centre, University of Edinburgh, Edinburgh, UK.

[3]MRC London Institute of Medical Sciences, Institute of Clinical Sciences, Imperial College London, UK

[§]Authors for correspondence: steven.pollard@ed.ac.uk and tristan.rodriguez@imperial.ac.uk

Running title: Glioblastoma stem cell competition

Keywords: Neural stem cells, quiescence, glioblastoma, Notch, cell competition

Abstract

There is increasing evidence demonstrating that adult neural stem cells (NSCs) are a cell of origin of glioblastoma. Here we have analysed the interaction between transformed and wild-type NSCs isolated from the adult mouse subventricular zone niche. We find that transformed NSCs are refractory to quiescence-inducing signals. Unexpectedly, we also demonstrate that these cells induce quiescence in surrounding wild-type NSCs in a cell-cell contact and Notch signalling-dependent manner. Our findings therefore suggest that oncogenic mutations are propagated in the stem cell niche not just through cell-intrinsic advantages, but also by outcompeting neighbouring stem cells through repression of their proliferation.

Introduction

In the adult mammalian brain, neural stem cells (NSCs) can be primarily found in specific neurogenic regions. In rodents these include the sub-granular zone (SGZ) of the dentate gyrus (DG) and the subventricular zone (SVZ), which lines the lateral ventricles (Doetsch et al. 1999; Sanai et al. 2004; Quinones-Hinojosa et al. 2006). In the SVZ niche NSCs coexist in both quiescent and activated states (Quinones-Hinojosa et al. 2006). Tight regulation of the switch between these two states is vital to ensure that the pool of NSCs does not accumulate DNA damage or become exhausted with time, and therefore understanding how this is achieved is of great interest. The feedback mechanisms that exist to regulate the balance of stem cell activation and quiescence during normal homeostasis remain poorly understood.

Adult NSCs are believed to be a cell of origin in certain brain tumours. One possibility is that these cells accumulate driver mutations over time that compromise the normal controls on their proliferation and migration. These transformed NSCs then escape the niche and acquire further mutations resulting in tumour formation. This has been hypothesised to be the case in glioblastoma (GBM), the most aggressive form of malignant glioma (Louis et al. 2007; Rispoli et al. 2014). In particular, the discovery of a subpopulation of cells within GBM tumours with stem cell characteristics, known as glioblastoma stem cells (GSCs), has lent weight to this notion. This GSC population shares many common features with adult NSCs, including expression of stem and progenitor cell markers, self-renewal capacity, and the ability to generate multilineage progeny (Singh et al. 2004; Cheng et al. 2013). Importantly, GSCs are also able to generate tumours in mice that recapitulate all the classical features of GBM, even when injected in low numbers (Galli et al. 2004; Singh et al. 2004).

Adult NSCs can be isolated from the SVZ of murine brains and cultured as adherent cultures under conditions that promote symmetric self-renewal and prevent differentiation (Conti et al. 2005; Pollard et al. 2006). Furthermore, by using NSCs engineered with oncogenic drivers, these *in vitro* culture systems can be useful as a model of brain tumour development to understand cellular transformation. Here we exploit this system to understand how transformed NSCs influence wild-type NSCs.

Results and Discussion

Transformed NSCs are refractory to quiescence-inducing signals.

To understand how transforming mutations affect the quiescent or activation status of NSCs, we compared NSCs derived from wild-type mice (WT-NSCs) to those isolated from *Ink4a/Arf* $^{-/-}$ mice and transduced with a retrovirus expressing the EGFRvIII mutation (IE-NSCs) (Bruggeman et al. 2007). This combination of mutations is frequently observed in human GBM (Crespo et al. 2015) and induces transformation in NSCs, as indicated by their ability to generate tumours *in vivo* that recapitulate many of the features of human GBM tumours (Bruggeman et al. 2007; Marques-Torrejon et al. 2018). We first compared the proliferative potential of both these cell types. We observed that, when grown in conditions that promote the proliferative NSC state (Pollard et al. 2006), IE-NSCs displayed a small growth advantage (Figure 1A and Supplemental Fig. S1A-B). We next investigated if IE-NSCs have a similar response to quiescence-inducing signals when compared to WT-NSCs. BMP signalling is known to induce a reversible quiescent-like state in hippocampal and embryonic stem cell-derived NSCs (Mira et al. 2010; Martynoga et al. 2013). For this reason, we treated WT and IE-NSCs with 50ng/ml BMP4. We observed that, although this induced similar levels of SMAD1/5/8 phosphorylation in both cell types (Supplemental Fig. S1C) and efficiently suppressed the proliferation of WT-NSCs, it had little effect on the growth of the transformed cells (Supplemental Fig. S1D). This suggests that IE-NSCs cells are refractory to the induction of quiescence by BMP signalling activation.

Transformed NSCs suppress the proliferation of surrounding NSCs.

The experiments described above allowed us to test the proliferative potential of wild-type and transformed cells as isolated cell populations. However, we postulated that in the niche these cell types are likely to co-exist. For this reason, we next studied the proliferation patterns of both cell types in a 50:50 co-culture and compared these proliferative patterns to the growth of cell populations in homotypic (separate) cultures.

IE-NSCs were GFP-labelled, allowing us to accurately quantify the relative cell proliferation rates in co-culture using flow cytometry. Given transformed cells produce autocrine and paracrine growth factors, these might support increased WT-NSC expansion. Unexpectedly however, we observed that in contrast to the exponential growth observed for both cell types in separate culture, in co-culture WT-NSCs showed a significant reduction in the rate of proliferation (Figure 1B-E and Supplemental Fig. S1E-F). These results suggest that IE-NSCs have an acquired inhibitory effect on the proliferation of WT-NSCs.

To test the above possibility further, co-cultures were established with varying proportions of each cell type, ranging from 10 to 90%, and the total number of cells present in co-culture was kept constant. Analysis of the fold change in WT-NSC number, which normalises for variations in WT-NSC numbers at initial plating, revealed that the reduction in their proliferation was directly proportional to the percentage of transformed NSCs present (Figure 1F), to the extent that, when 75% of the cells in co-culture were IE-NSCs, the 25% of WT-NSCs barely increased in number during the 6-day experiment. Interestingly, cleaved-Caspase3 expression was also

elevated in co-cultured WT-NSCs (Supplemental Fig. S1G). However, this increase was only significant from day 5 of co-culture when compared to separate cultures. Given that the differences in cell number and BrdU incorporation were apparent from day 3, this suggests that apoptosis may be due to the compromised ability of arrested NSCs to survive long-term in pro-proliferative conditions. Together, these results indicate that IE-NSCs suppress the proliferation of activated WT-NSCs.

Transformed NSCs induce a quiescent-like state in neighbouring wild-type NSCs

To gain a deeper insight into the mechanism of proliferative arrest of co-cultured WT-NSCs, we compared their transcriptional profile to WT-NSCs grown in separate cultures. Cells were isolated by FACS after 5 days of co-culture, and RNA-seq was performed. Analysis of differential gene expression with Ingenuity Pathway Analysis, which uses functional annotations and interactions of genes to identify enriched pathways, revealed that the majority of the top canonical pathways enriched in co-cultured WT-NSCs were related to cell cycle control and DNA repair (Figure 2A-B), consistent with the observed proliferation arrest induced by transformed cells.

One possible explanation for this cell cycle arrest is differentiation into post-mitotic cell types, such as immature neurons. The expression of NSC markers, together with markers for intermediate progenitors and differentiated cell types (Zhang and Jiao 2015), was therefore explored in our RNA-seq data-set. No broad downregulation of classical NSC markers or any upregulation of differentiation markers was observed in co-cultured WT-NSCs compared to their separate counterparts (Supplemental Fig. S2A). Interestingly, we did observe an upregulation in the expression of the glial markers, *Gfap, Glt1* and *Glast*, which are enriched in quiescent NSCs (Codega et al. 2014; Llorens-Bobadilla et al. 2015). These observations suggest that WT-NSCs are not differentiating, but instead may be driven into a quiescent astrocytic-like state.

To explore this last possibility, we analysed our RNA-seq data-set for the expression of a broader set of quiescent and activated NSC markers. We found that the quiescence-associated transcriptional regulators, *Sox9*, *Id2*, *Id3* and *Klf9,* which are upregulated in quiescent SVZ NSCs (Llorens-Bobadilla et al. 2015; Morizur et al. 2018), were all also upregulated in the co-cultured WT-NSCs (Figure 2C). We also observed that markers of activated NSCs, *Ascl1*, *Egr1*, *Fos* and *Sox11* (Andersen et al. 2014; Llorens-Bobadilla et al. 2015; Morizur et al. 2018), were downregulated in these cells. When we compared our RNA-seq data-set with a list of transcription factors and co-factors that have been found to be differentially expressed between activated and quiescent SVZ NSCs (Morizur et al. 2018), we found that of the 14 genes enriched in quiescent cells in this study, 10 were upregulated in co-cultured WT-NSCs, and of the 61 genes enriched in activated NSCs, 50 were downregulated (Supplemental Fig. S2B). Together these findings therefore support the hypothesis that the co-cultured NSCs are adopting a quiescent phenotype.

To test if the quiescent WT-NSCs remain multipotent after co-culture with transformed NSCs, we co-cultured both these cell types for 5 days, sorted the WT-NSCs and then re-plated them

in differentiation inducing conditions. When this was done, we observed that the co-cultured WT-NSCs had a similar ability to differentiate into astrocytes, neural progenitors and neurons as separately cultured WT-NSCs did (Figure 2D-E and Supplemental Fig. S2C-D). This indicates that the co-cultured quiescent NSCs retain multipotency.

A key feature of a quiescent phenotype is its reversibility. To test if the proliferation arrest of WT-NSCs in co-culture is reversible, we sorted WT and IE-NSCs after 5 days in co-culture and re-plated them. In parallel, WT-NSCs that had been cultured separately were mixed with transformed cells just before sorting and subsequently re-plated. Importantly, we observed that previously co-cultured WT-NSCs displayed a similar proliferation rate to NSCs that had been separately cultured throughout, as judged by their growth curves and BrdU incorporation (Figure 2F-G). The reversible nature of the proliferation arrest of co-cultured WT-NSCs provides further evidence that they are entering a quiescent state rather than becoming senescent or terminally differentiated.

Cell contact is required for the inhibitory effect of transformed cells

To understand the mechanisms underlying the interaction between WT and transformed NSCs, we first analysed the possible involvement of the mTOR signalling pathway. mTOR is a metabolic regulator that senses growth factor and nutrient inputs. It is activated in transit amplifying progenitor cells and its inhibition induces quiescence in adult NSCs (Paliouras et al. 2012). Analysis of the expression of ribosomal protein S6 phosphorylation (p-S6), a read-out of mTOR activity indicated that mTOR signalling levels were reduced in co-cultured WT-NSCs, not only relative to these same cells in separate culture, but also to IE-NSCs in co-culture (Figure 3A). We next tested if constitutive mTOR activation was sufficient to prevent these NSCs from entering quiescence in co-culture. For this we mutated *Tsc2*, an mTOR repressor in WT-NSCs, using CRISPR-Cas9 targeting (Supplemental Fig. S3A). However, we found that, although this was sufficient to sustain strong mTOR pathway activation, *Tsc2*$^{-/-}$ NSCs still entered a proliferation arrest when co-cultured with IE-NSCs (Supplemental Fig. S3B-D). This indicates that mTOR inhibition is not the primary event for the induction of quiescent phenotype of co-cultured WT-NSCs.

Next, we investigated the possibility that cell contact is required to induce the growth arrest of WT-NSCs. We first used a transwell assay, where the two cell types are separated by a permeable membrane that allows the exchange of signalling factors in the media while physically separating the cells. When WT-NSCs were separated from IE-NSCs by the transwell, they grew similarly to WT-NSCs in homotypic cultures (Figure 3B). This suggests that secreted paracrine factors are not sufficient to induce quiescence. We further tested this possibility by using fences, which are metal inserts that divide the well into an inner and outer ring. One cell type is plated in the inner ring and the second in the outer ring (Figure 3C) and once they are growing adherently, the inserts can be removed leaving behind a small gap between the two populations. Using this system, we compared the proliferation rate of WT-NSCs that were separated from IE-NSCs to their proliferation when separated from other WT-NSCs or when mixed with IE-NSCs. We found that the rate of BrdU incorporation of the WT-

NSCs did not decrease when they were not in physical contact with the IE-NSCs (Figure 3C). This indicates that cell-cell contact is most likely required for IE-NSCs to inhibit the proliferation of WT-NSCs.

Transformed cells signal via Notch and Rbpj to induce quiescence in wild-type NCSs

The Notch pathway is a highly conserved signalling pathway requiring cell-cell contact that plays a central role in the regulation of embryonic and adult neurogenesis (Ables et al. 2011; Urban and Guillemot 2014). To test if Notch signalling is required to trigger quiescence, we first explored the expression of Notch signalling pathway components in our RNA-seq data. Interestingly, we found that the majority of Notch-related genes were upregulated in WT-NSCs compared to IE-NSCs, including many Notch targets and receptors, while the Notch ligands appeared to be more highly expressed on IE-NSCs in co-culture (Figure 3D). With the exception of *Jagged1*, this higher expression of Notch ligands in IE-NSCs was not dependent on their co-culture with WT-NSCs (Supplemental Fig. S4A), suggesting that cell-cell communication was not driving this initial difference in expression. Analysis by qPCR of sorted samples also revealed that the expression of the Notch target genes *Hes1, Hes5, Hes7, Hey1, Hey2* and *Nrarp* were upregulated in co-cultured WT-NSCs (Figure 3E). This suggests that Notch pathway activity is higher in co-cultured WT-NSCs than in IE-NSCs and raises the possibility that transformed cells may be signalling to WT-NSCs via this pathway.

To test the functional significance of this difference in Notch activation, two complementary γ-secretase inhibitors were used to block Notch signalling. We observed that both LY411575 (LY) and crenigacestat reduced Notch target gene expression in NSCs. Importantly, these also partially rescued the proliferation arrest of co-cultured WT-NSCs. The growth curves and BrdU incorporation rates of co-cultured NSCs treated with the γ-secretase inhibitors were only slightly lower than their growth is separate culture (Figure 3F-G and Supplemental Fig. S4B-F). This suggests that Notch signalling is required for the induction of quiescence in NSCs by transformed cells.

To further test the requirement for Notch signalling we mutated *Rbpj*, a key effector of this pathway, as well as *Notch1* and *Notch2* by CRISPR/Cas9 targeting (Figure 4A, D and G). *Rbpj*$^{-/-}$, *Notch1*$^{-/-}$ or *Notch2*$^{-/-}$ NSCs were not susceptible to proliferation arrest when co-cultured with IE-NSCs and grew at similar growth rates in separate and co-culture (Supplemental Fig. S5A-D). Similarly, the fold change in cell number and BrdU incorporation rates of co-cultured *Rbpj*$^{-/-}$, *Notch1*$^{-/-}$ and *Notch2*$^{-/-}$ NSCs was similar to separate culture and significantly higher than that of WT-NSCs co-cultured with IE-NSCs (Figure 4B-C, E-F and H-I). Interestingly, both the growth curves and final cell counts of *Rbpj*$^{-/-}$ NSCs indicated that these cell types even outcompeted IE-NSCs in co-culture (Figure 4B and Supplemental Fig. S5B), suggesting that disrupting Notch signalling may be sufficient to provide NSCs with a competitive advantage against transformed NSCs. The ability of both *Notch1* and *Notch2* deletion to render the NSCs insensitive to proliferation arrest suggests that these receptors both have a role in conveying the quiescence-inducing signal to WT NSCs. This is in contrast to recent studies that have suggested a non-redundant role for Notch2 in promoting NSC quiescence (Engler et al. 2018).

It would also suggest that it is not necessary to completely block Notch signalling to prevent growth arrest, reducing the strength of the signal through deletion of a single receptor was sufficient.

To exclude the possibility that Notch signalling is required in transformed NSCs, we mutated *Rbpj* in this cell type (Supplemental Fig. S5E). We observed that IE-NSCs still induced the proliferation arrest of WT-NSCs, as shown by the growth curves, final cell numbers and BrdU incorporation (Supplemental Fig. S5F-H). Therefore, Notch signalling is not required in transformed cells for their growth inhibition of WT-NSCs.

Finally, to test if cells carrying other mutations that induce transformation can also induce quiescence in WT-NSCs we analysed *Pten*$^{-/-}$; *p53*$^{-/-}$ NSCs, that when mutated in mice induce a glioblastoma-like phenotype (Zheng et al. 2008; Jacques et al. 2010). Mutant NSCs were generated by CRISPR/Cas9 targeting and cultured separately or co-cultured with WT-NSCs. Indeed, *Pten*$^{-/-}$; *p53*$^{-/-}$ NSCs were capable of inducing a growth arrest in WT-NSCs (Supplemental Fig. S6). The ability to induce quiescence in neighbouring cells is therefore not dependent on the specific IENS model, but may be a common feature of several different types of transformed NSCs.

Altogether, these data, demonstrate that transformed cells activate Notch signalling in adjacent wild-type activated NSCs and triggers transition to quiescence. This observation may have implications for understanding of gliomagenesis. In humans, it has been suggested that GBMs can arise from the adult SVZ cells and accumulate low-level truncal driver mutations (Lee et al. 2018). This niche has also been suggested to harbour malignant cells away from the tumour mass, which are more resistant to chemotherapy and may therefore act as a reservoir for recurrence (Piccirillo et al. 2015). Furthermore, the SVZ has been shown to be a permissive region for GBM growth, as tumours in contact with this region are associated with decreased patient survival and increased recurrence (Khalifa et al. 2017; Mistry et al. 2017).

Our studies using SVZ-derived wild-type and transformed NSCs demonstrate that transformed cells provide a negative feedback via Notch signalling to surrounding normal NSCs, which cause them to exit their activated state and re-enter quiescence. By this mechanism, oncogenic NSCs outcompete normal NSCs and ensure their preferential self-renewal and differentiation, therefore increasing both their cell number and their likelihood of giving rise to progenitor cells and exiting the niche. This competitive advantage may be an important early step in the development of glioma and GBM. Confirming and tracking quiescent NSCs *in vivo* and establishing how this competition mechanism operates in the complex milieu of the SVZ niche are important future directions to understand the aetiology of GBM.

Material and Methods

Neural Stem Cell Cultures

Adult murine NSCs were derived from the SVZ by the protocol described in (Conti et al. 2005; Pollard et al. 2006). Transformed *Ink4a/Arf*$^{-/-}$; EGFRvIII NSCs (IE-NSCs) were previously generated by the Maarten van Lohuizen laboratory (Netherlands Cancer Institute, NKI). NSCs were isolated from *Ink4a/Arf*$^{-/-}$ mice and transduced with EGFRvIII pMSCV retrovirus (Bruggeman et al. 2007).

Co-culture assays

40,000 cells per well were seeded in a 24-well plate either separately or as a 50:50 mix of WT and IE-NSCs. The proportion of each cell type was assessed by determining the percentage of GFP-positive cells by flow cytometry performed on an LSR-II Analyser (BD Biosciences).

Differentiation of NSCs

Sorting was performed by FACS at day five of the six-day assay for three biological repeats. Cells were seeded onto coverslips in NSC media for 24 hours following sorting. Media was then replaced for either NSC media with 10% FCS or NSC media without EGF addition. Media was replaced every other day and cells were fixed after 4 days in FCS or 6 days without EGF.

Flow cytometry immunolabelling

Cells were fixed in 2% formaldehyde and permeabilised in ice-cold 90% methanol. For BrdU analysis, cells were incubated with BrdU for 2 hours prior to fixation. Cells were then incubated with DNaseI prior to blocking. Primary antibodies (p-S6, cleaved-Caspase3 or BrdU, CST 1:200) were detected with AlexFluor 546 secondary antibodies (Molecular Probes). Flow cytometry was performed on an LSR-II Analyser (BD Biosciences) and data analysed with the FlowJo software.

RNA-sequencing analysis

Sorting was performed by FACS at day 5 of the 6-day assay for 3 biological repeats. mRNA was isolated, fragmented, converted to cDNA and ligated to Illumina adapters. Sequencing was performed using the HiSeq 4000 system (Illumina). Differential expression was determined using the DESeq2 package (Love et al. 2014) and the resulting gene sets were analysed using IPA software (Qiagen)(Kramer et al. 2014). A 'Core Analysis' was performed for each comparison on genes differentially expressed with a false discovery rate of less than 10%.

CRISPR gene targeting of NSCs

gRNAs for targeting of *Rbpj, Notch1*, *Notch2* and *P53*$^{-/-}$ were cloned into the pX330-U6-Chimeric_BB-CBh-hSpCas9 (PX330) expression plasmid (gift from Feng Zhang, Addgene plasmid #42230) as previously described (Ran et al. 2013). Details of *Tsc2*$^{-/-}$ NSC generation can be found in Supplemental Methods and gRNA sequences in Supplemental Table 2. NSCs were transfected with 2µg plasmid DNA and 0.125µg Puro-pPYCAGIP vector or linear hygromycin marker (Clontech 631625) by nucleofection (AMAXA 2B, Lonza). Selection was performed from 48 hours post-transfection until the emergence of resistant colonies. *Pten*$^{-/-}$

NSCs were generated as described in (Bressan et al. 2017) and then transfected with gRNAs targeting *P53* as described above.

Quantification and Statistical Analysis

Statistical analysis and data representation were performed using GraphPad Prism software. Statistical methods used and sample size (n) are indicated in the relevant figure legends. Adjusted p values are displayed as * $p<0.05$, ** $p<0.01$ and *** $p<0.001$.

Data availability

The raw data for the RNA-sequencing of wild-type and transformed NSCs have been deposited in the arrayexpress database under accession number E-MTAB-8580.

Acknowledgments

We would like to thank Stephen Rothery in the Facility for Imaging by Light Microscopy (FILM) at Imperial College London for guidance and advice with confocal microscopy. Gratitude also goes to James Elliot and Roberta Maggio from the LMS/NIHR Imperial Biomedical Research Centre Flow Cytometry Facility for performing cell sorts. IENS cells were generously provided by Maarten van Lohuizen (NKI, Amsterdam). Steven Pollard is supported by a Cancer Research UK Senior Fellowship (A17368). Research in the Rodriguez lab was supported by the MRC project grant (MR/N009371/1), by the Rosetrees Trust grant (M693) and by the British Heart Foundation centre for research excellence. Katerina Lawlor was supported by an NHLI PhD studentship.

Conflicts of interests

The authors declare no competing financial or non-financial interests. Steven Pollard is founder and shareholder of Cellinta.

Figure Legends

Figure 1. **WT-NSCs show reduced proliferation in the presence of transformed NSCs.** **(A)** Growth curves of WT and IE-NSCs cultured separately or **(B)** co-cultured over 6 days. N>10, ANOVA followed by Sidak's multiple comparisons test. (**C)** Quantification of fold change in cell number relative to seeding density for each culture condition. N>10, ANOVA followed by Sidak's multiple comparisons test. **(D)** Proportion of BrdU-positive cells in each culture condition at day 5 following a 2-hour BrdU chase. N=10, ANOVA followed by Sidak's multiple comparisons test. **(E)** Representative immunoblot for phospho-histone-3 (p-H3) in WT-NSCs sorted at day 5 and quantification of p-H3 expression relative to β-actin. N=3, Student's paired T test. **(F)** Fold change cell number of WT-NSCs cultured in co-cultures with varying proportions of IE-NSCs. N=3.

Figure 2. WT-NSCs adopt a quiescent phenotype in the presence of transformed NSCs. **(A)** Top canonical pathways, **(B)** changes in cell cycle gene expression and **(C)** changes in quiescence and activation-associated gene expression in WT-NSCs in co-culture versus separate culture revealed by RNA-seq. N=3. **(D)** Immunofluorescence images and **(E)**

quantification of WT-NSCs stained with GFAP or BIII-Tubulin after being grown separately or in co-culture, then sorted and re-plated in differentiation inducing conditions. N=3, 2-way ANOVA followed by Sidak's multiple comparisons test. **(F)** Growth curves and **(G)** proportion of BrdU-positive WT-NSCs after being grown separately or in co-culture and then sorted and re-plated. N=3.

Figure 3. Quiescence of WT- NSCs is induced by direct contact with transformed NSCs and is associated with increased Notch activation

(A) Flow cytometry plot showing p-S6 staining in WT and transformed NSCs in separate and co-culture and quantification of median fluorescence intensity. N=6, ANOVA followed by Sidak's multiple comparisons test. **(B)** Growth curves of WT-NSCs cultured below transwell inserts with WT, transformed or mixed cultures. N=3. **C** Percentage of BrdU-positive WT-NSCs from the inner ring of the three different cultures shown. N=3, one-way ANOVA followed by Tukey's multiple comparisons test. **(D)** Heat map showing changes in Notch gene expression after RNA-seq and **(E)** after RT-qPCR in co-cultured transformed and WT-NSCs. N=3, 2-way ANOVA followed by Sidak's multiple comparisons test. **(F)** Quantification of the fold change in NSC number after separate or co-culture with transformed cells (N=8) and **(G)** proportion of BrdU positive cells with and without addition of LY411575. N=4.

Figure 4. **Disruption of Notch signalling rescues WT- NSC proliferation in co-culture.**

(A, D, G) Western blot showing absence of RBPJ protein in *Rbpj*$^{-/-}$ clones (A), NOTCH1 protein in *Notch1*$^{-/-}$ clones (D) and NOTCH2 protein in *Notch2*$^{-/-}$ clones (G). **(B, E, H)** Fold change cell number quantification and **(C, F, I)** proportion of BrdU-positive cells in EV and *Rbpj*$^{-/-}$ NSCs in separate and co-culture with transformed NSCs (B) N=4 (C) N=5; in EV and *Notch1*$^{-/-}$ NSCs in separate and co-culture with transformed NSCs (E) N=4 (F) N=5; and in EV and *Notch2*$^{-/-}$ NSCs in separate and co-culture with transformed NSCs (H) N=4 (I) N=5. 2-way ANOVA followed by Sidak's multiple comparisons test.

References

Ables JL, Breunig JJ, Eisch AJ, Rakic P. 2011. Not(ch) just development: Notch signalling in the adult brain. *Nat Rev Neurosci* **12**: 269-283.

Andersen J, Urban N, Achimastou A, Ito A, Simic M, Ullom K, Martynoga B, Lebel M, Goritz C, Frisen J et al. 2014. A transcriptional mechanism integrating inputs from extracellular signals to activate hippocampal stem cells. *Neuron* **83**: 1085-1097.

Bressan RB, Dewari PS, Kalantzaki M, Gangoso E, Matjusaitis M, Garcia-Diaz C, Blin C, Grant V, Bulstrode H, Gogolok S et al. 2017. Efficient CRISPR/Cas9-assisted gene targeting enables rapid and precise genetic manipulation of mammalian neural stem cells. *Development* **144**: 635-648.

Bruggeman SW, Hulsman D, Tanger E, Buckle T, Blom M, Zevenhoven J, van Tellingen O, van Lohuizen M. 2007. Bmi1 controls tumor development in an Ink4a/Arf-independent manner in a mouse model for glioma. *Cancer Cell* **12**: 328-341.

Cheng L, Huang Z, Zhou W, Wu Q, Donnola S, Liu JK, Fang X, Sloan AE, Mao Y, Lathia JD et al. 2013. Glioblastoma stem cells generate vascular pericytes to support vessel function and tumor growth. *Cell* **153**: 139-152.

Codega P, Silva-Vargas V, Paul A, Maldonado-Soto AR, Deleo AM, Pastrana E, Doetsch F. 2014. Prospective identification and purification of quiescent adult neural stem cells from their in vivo niche. *Neuron* **82**: 545-559.

Conti L, Pollard SM, Gorba T, Reitano E, Toselli M, Biella G, Sun Y, Sanzone S, Ying QL, Cattaneo E et al. 2005. Niche-independent symmetrical self-renewal of a mammalian tissue stem cell. *PLoS Biol* **3**: e283.

Crespo I, Vital AL, Gonzalez-Tablas M, Patino Mdel C, Otero A, Lopes MC, de Oliveira C, Domingues P, Orfao A, Tabernero MD. 2015. Molecular and Genomic Alterations in Glioblastoma Multiforme. *Am J Pathol* **185**: 1820-1833.

Doetsch F, Caille I, Lim DA, Garcia-Verdugo JM, Alvarez-Buylla A. 1999. Subventricular zone astrocytes are neural stem cells in the adult mammalian brain. *Cell* **97**: 703-716.

Engler A, Rolando C, Giachino C, Saotome I, Erni A, Brien C, Zhang R, Zimber-Strobl U, Radtke F, Artavanis-Tsakonas S et al. 2018. Notch2 Signaling Maintains NSC Quiescence in the Murine Ventricular-Subventricular Zone. *Cell Rep* **22**: 992-1002.

Galli R, Binda E, Orfanelli U, Cipelletti B, Gritti A, De Vitis S, Fiocco R, Foroni C, Dimeco F, Vescovi A. 2004. Isolation and characterization of tumorigenic, stem-like neural precursors from human glioblastoma. *Cancer Res* **64**: 7011-7021.

Jacques TS, Swales A, Brzozowski MJ, Henriquez NV, Linehan JM, Mirzadeh Z, C OM, Naumann H, Alvarez-Buylla A, Brandner S. 2010. Combinations of genetic mutations in the adult neural stem cell compartment determine brain tumour phenotypes. *EMBO J* **29**: 222-235.

Khalifa J, Tensaouti F, Lusque A, Plas B, Lotterie JA, Benouaich-Amiel A, Uro-Coste E, Lubrano V, Cohen-Jonathan Moyal E. 2017. Subventricular zones: new key targets for glioblastoma treatment. *Radiat Oncol* **12**: 67.

Kramer A, Green J, Pollard J, Jr., Tugendreich S. 2014. Causal analysis approaches in Ingenuity Pathway Analysis. *Bioinformatics* **30**: 523-530.

Lee JH, Lee JE, Kahng JY, Kim SH, Park JS, Yoon SJ, Um JY, Kim WK, Lee JK, Park J et al. 2018. Human glioblastoma arises from subventricular zone cells with low-level driver mutations. *Nature* **560**: 243-247.

Llorens-Bobadilla E, Zhao S, Baser A, Saiz-Castro G, Zwadlo K, Martin-Villalba A. 2015. Single-Cell Transcriptomics Reveals a Population of Dormant Neural Stem Cells that Become Activated upon Brain Injury. *Cell Stem Cell* **17**: 329-340.

Louis DN, Ohgaki H, Wiestler OD, Cavenee WK, Burger PC, Jouvet A, Scheithauer BW, Kleihues P. 2007. The 2007 WHO classification of tumours of the central nervous system. *Acta Neuropathol* **114**: 97-109.

Love MI, Huber W, Anders S. 2014. Moderated estimation of fold change and dispersion for RNA-seq data with DESeq2. *Genome Biol* **15**: 550.

Marques-Torrejon MA, Gangoso E, Pollard SM. 2018. Modelling glioblastoma tumour-host cell interactions using adult brain organotypic slice co-culture. *Dis Model Mech* **11**.

Martynoga B, Mateo JL, Zhou B, Andersen J, Achimastou A, Urban N, van den Berg D, Georgopoulou D, Hadjur S, Wittbrodt J et al. 2013. Epigenomic enhancer annotation reveals a key role for NFIX in neural stem cell quiescence. *Genes Dev* **27**: 1769-1786.

Mira H, Andreu Z, Suh H, Lie DC, Jessberger S, Consiglio A, San Emeterio J, Hortiguela R, Marques-Torrejon MA, Nakashima K et al. 2010. Signaling through BMPR-IA regulates quiescence and long-term activity of neural stem cells in the adult hippocampus. *Cell Stem Cell* **7**: 78-89.

Mistry AM, Hale AT, Chambless LB, Weaver KD, Thompson RC, Ihrie RA. 2017. Influence of glioblastoma contact with the lateral ventricle on survival: a meta-analysis. *J Neurooncol* **131**: 125-133.

Morizur L, Chicheportiche A, Gauthier LR, Daynac M, Boussin FD, Mouthon MA. 2018. Distinct Molecular Signatures of Quiescent and Activated Adult Neural Stem Cells Reveal Specific Interactions with Their Microenvironment. *Stem Cell Reports* **11**: 565-577.

Paliouras GN, Hamilton LK, Aumont A, Joppe SE, Barnabe-Heider F, Fernandes KJ. 2012. Mammalian target of rapamycin signaling is a key regulator of the transit-amplifying progenitor pool in the adult and aging forebrain. *J Neurosci* **32**: 15012-15026.

Piccirillo SG, Spiteri I, Sottoriva A, Touloumis A, Ber S, Price SJ, Heywood R, Francis NJ, Howarth KD, Collins VP et al. 2015. Contributions to drug resistance in glioblastoma derived from malignant cells in the sub-ependymal zone. *Cancer Res* **75**: 194-202.

Pollard SM, Conti L, Sun Y, Goffredo D, Smith A. 2006. Adherent neural stem (NS) cells from fetal and adult forebrain. *Cereb Cortex* **16 Suppl 1**: i112-120.

Quinones-Hinojosa A, Sanai N, Soriano-Navarro M, Gonzalez-Perez O, Mirzadeh Z, Gil-Perotin S, Romero-Rodriguez R, Berger MS, Garcia-Verdugo JM, Alvarez-Buylla A. 2006. Cellular composition and cytoarchitecture of the adult human subventricular zone: a niche of neural stem cells. *J Comp Neurol* **494**: 415-434.

Ran FA, Hsu PD, Wright J, Agarwala V, Scott DA, Zhang F. 2013. Genome engineering using the CRISPR-Cas9 system. *Nat Protoc* **8**: 2281-2308.

Rispoli R, Conti C, Celli P, Caroli E, Carletti S. 2014. Neural stem cells and glioblastoma. *Neuroradiol J* **27**: 169-174.

Sanai N, Tramontin AD, Quinones-Hinojosa A, Barbaro NM, Gupta N, Kunwar S, Lawton MT, McDermott MW, Parsa AT, Manuel-Garcia Verdugo J et al. 2004. Unique astrocyte ribbon in adult human brain contains neural stem cells but lacks chain migration. *Nature* **427**: 740-744.

Singh SK, Hawkins C, Clarke ID, Squire JA, Bayani J, Hide T, Henkelman RM, Cusimano MD, Dirks PB. 2004. Identification of human brain tumour initiating cells. *Nature* **432**: 396-401.

Urban N, Guillemot F. 2014. Neurogenesis in the embryonic and adult brain: same regulators, different roles. *Front Cell Neurosci* **8**: 396.

Zhang J, Jiao J. 2015. Molecular Biomarkers for Embryonic and Adult Neural Stem Cell and Neurogenesis. *Biomed Res Int* **2015**: 727542.

Zheng H, Ying H, Yan H, Kimmelman AC, Hiller DJ, Chen AJ, Perry SR, Tonon G, Chu GC, Ding Z et al. 2008. p53 and Pten control neural and glioma stem/progenitor cell renewal and differentiation. *Nature* **455**: 1129-1133.

Figure 1

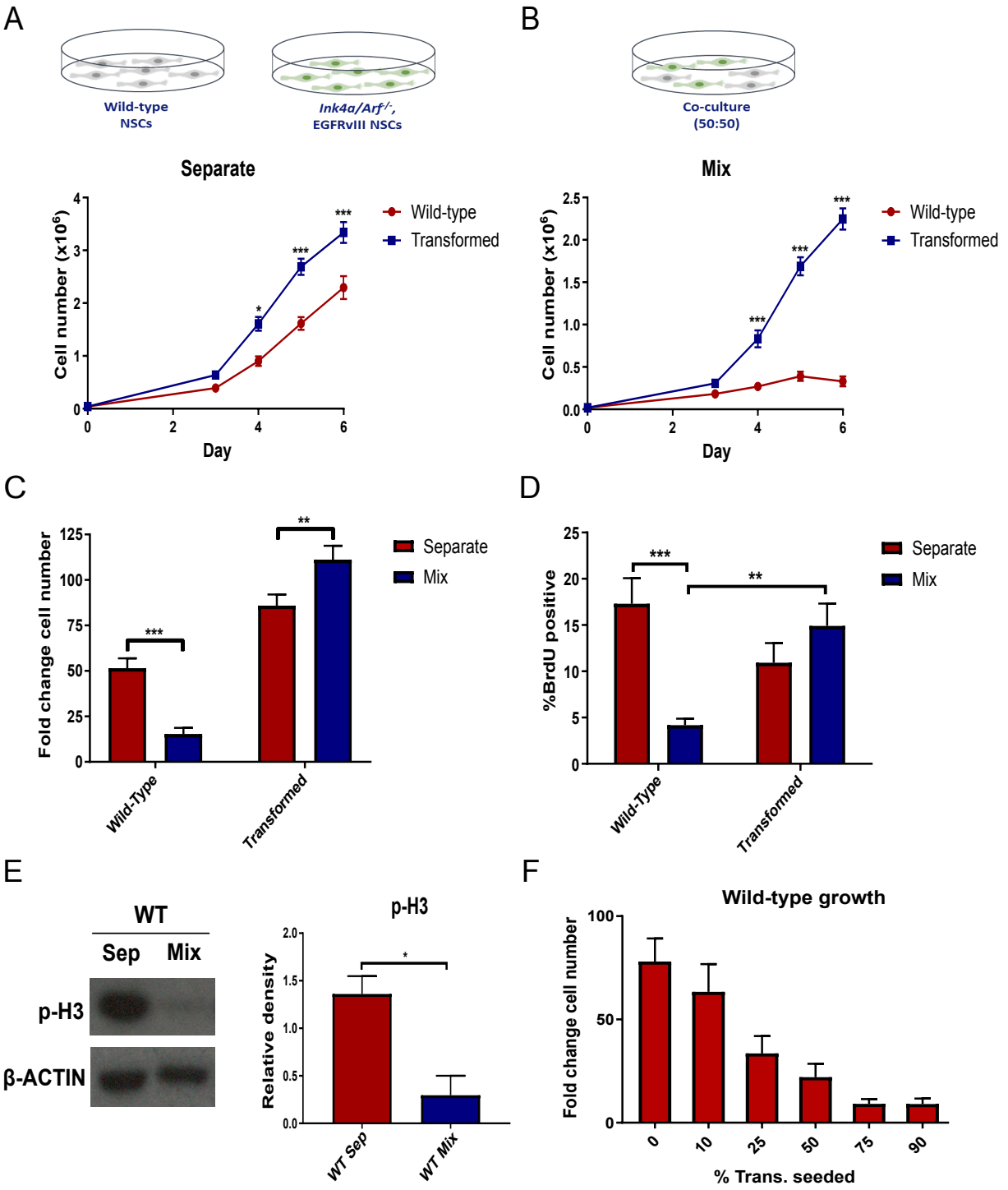
A
Wild-type NSCs
Ink4a/Arf-/-, EGFRvIII NSCs
Separate
Cell number (x10^6)
Day
Wild-type
Transformed
B
Co-culture (50:50)
Mix
Cell number (x10^6)
Day
Wild-type
Transformed
C
Fold change cell number
Separate
Mix
Wild-Type
Transformed
D
%BrdU positive
Separate
Mix
Wild-Type
Transformed
E
WT
Sep
Mix
p-H3
β-ACTIN
p-H3
Relative density
WT Sep
WT Mix
F
Wild-type growth
Fold change cell number
% Trans. seeded

Figure 2

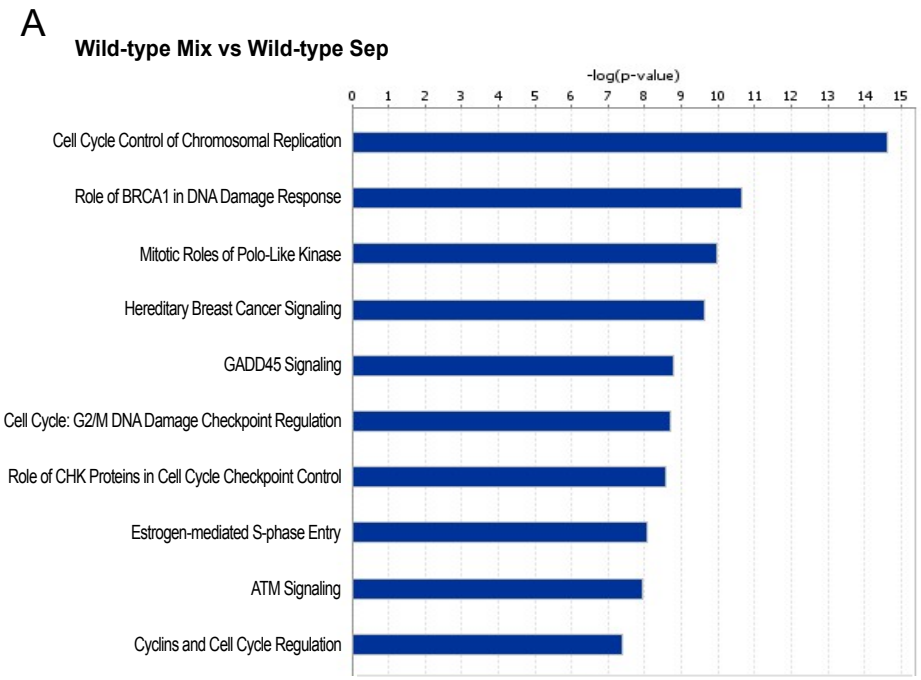
A
Wild-type Mix vs Wild-type Sep
-log(p-value)
0 1 2 3 4 5 6 7 8 9 10 11 12 13 14 15
Cell Cycle Control of Chromosomal Replication
Role of BRCA1 in DNA Damage Response
Mitotic Roles of Polo-Like Kinase
Hereditary Breast Cancer Signaling
GADD45 Signaling
Cell Cycle: G2/M DNA Damage Checkpoint Regulation
Role of CHK Proteins in Cell Cycle Checkpoint Control
Estrogen-mediated S-phase Entry
ATM Signaling
Cyclins and Cell Cycle Regulation

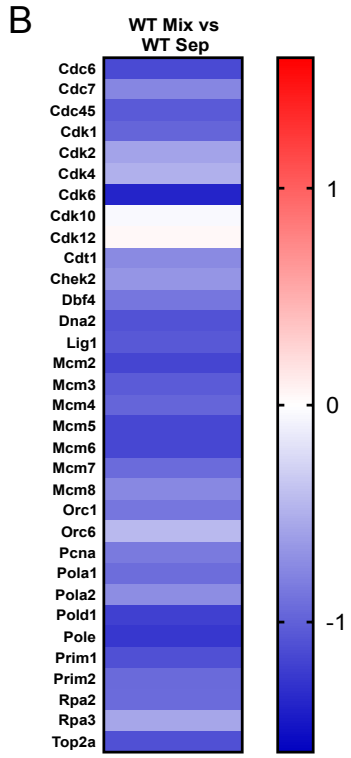
B
WT Mix vs WT Sep
Cdc6
Cdc7
Cdc45
Cdk1
Cdk2
Cdk4
Cdk6
Cdk10
Cdk12
Cdt1
Chek2
Dbf4
Dna2
Lig1
Mcm2
Mcm3
Mcm4
Mcm5
Mcm6
Mcm7
Mcm8
Orc1
Orc6
Pcna
Pola1
Pola2
Pold1
Pole
Prim1
Prim2
Rpa2
Rpa3
Top2a
1
0
-1

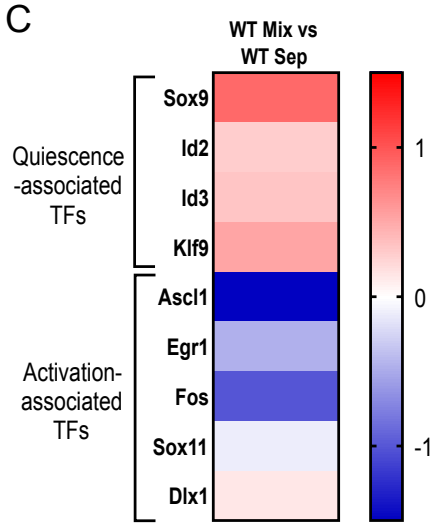
C
WT Mix vs WT Sep
Quiescence -associated TFs
Sox9
Id2
Id3
Klf9
Activation-associated TFs
Ascl1
Egr1
Fos
Sox11
Dlx1
1
0
-1

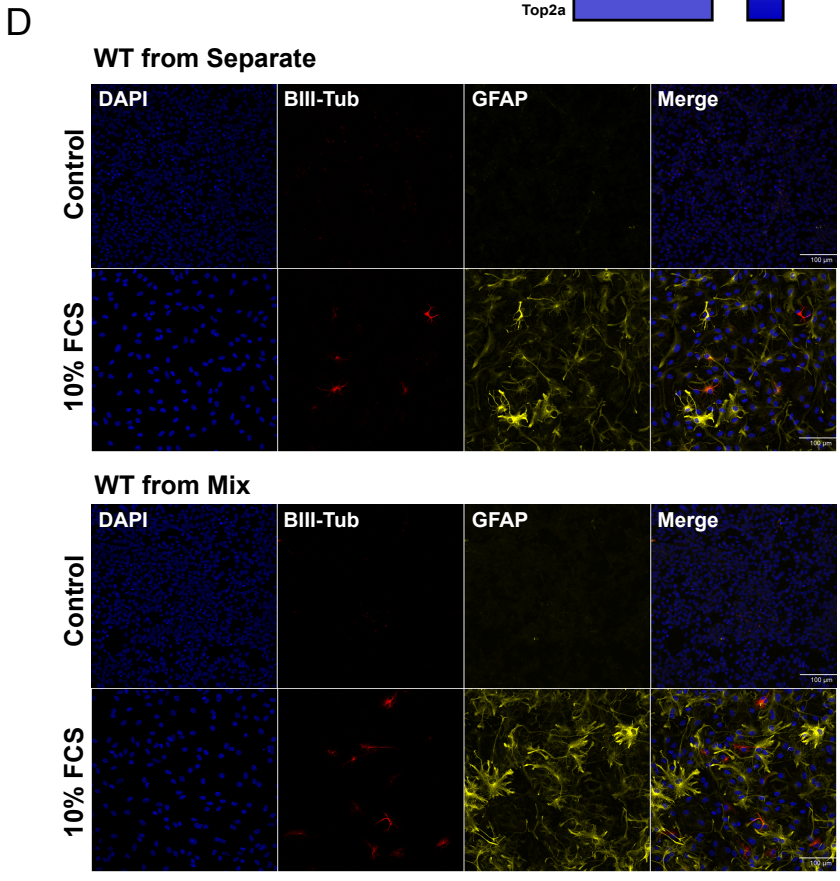
D
WT from Separate
DAPI
BIII-Tub
GFAP
Merge
Control
10% FCS
WT from Mix
DAPI
BIII-Tub
GFAP
Merge
Control
10% FCS

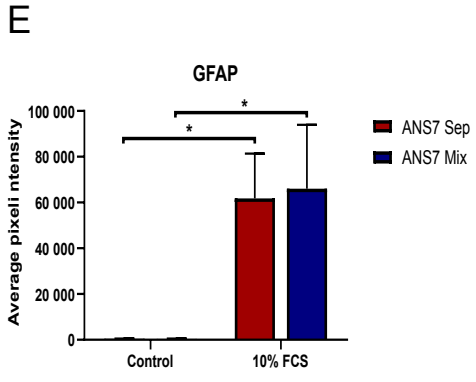
E
GFAP
Average pixeli ntensity
100 000
80 000
60 000
40 000
20 000
0
Control
10% FCS
ANS7 Sep
ANS7 Mix

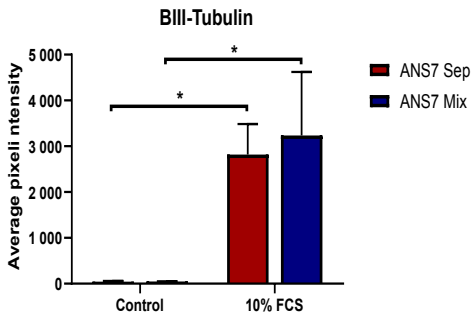
BIII-Tubulin
Average pixeli ntensity
5 000
4 000
3 000
2 000
1 000
0
Control
10% FCS
ANS7 Sep
ANS7 Mix

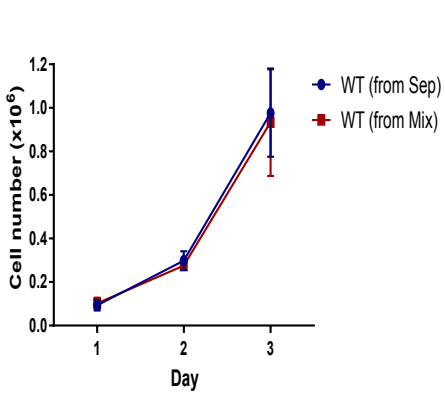
F
Cell number (x10⁶)
1.2
1.0
0.8
0.6
0.4
0.2
0.0
1
2
3
Day
WT (from Sep)
WT (from Mix)

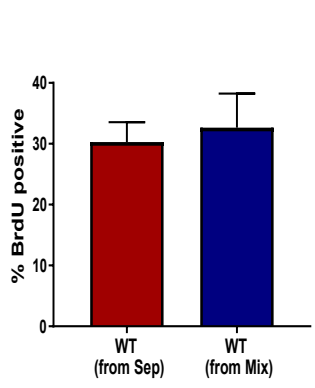
G
% BrdU positive
40
30
20
10
0
WT (from Sep)
WT (from Mix)

Figure 3

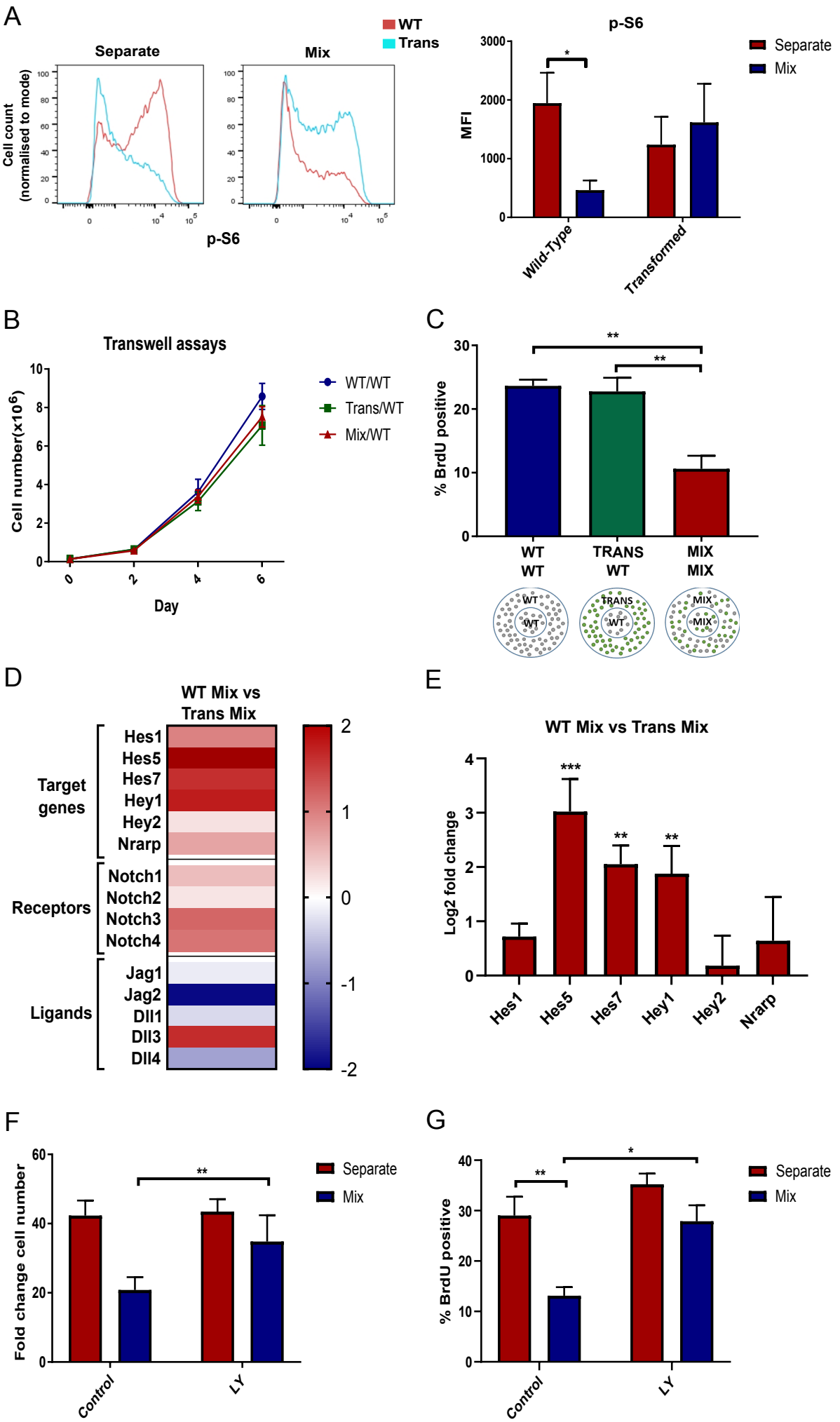
A
WT
Trans
Separate
Mix
Cell count (normalised to mode)
p-S6
p-S6
MFI
Separate
Mix
Wild-Type
Transformed
B
Transwell assays
Cell number(x10^6)
Day
WT/WT
Trans/WT
Mix/WT
C
% BrdU positive
WT WT
TRANS WT
MIX MIX
D
WT Mix vs Trans Mix
Target genes
Hes1
Hes5
Hes7
Hey1
Hey2
Nrarp
Receptors
Notch1
Notch2
Notch3
Notch4
Ligands
Jag1
Jag2
Dll1
Dll3
Dll4
E
WT Mix vs Trans Mix
Log2 fold change
Hes1
Hes5
Hes7
Hey1
Hey2
Nrarp
F
Fold change cell number
Separate
Mix
Control
LY
G
% BrdU positive
Separate
Mix
Control
LY

Figure 4

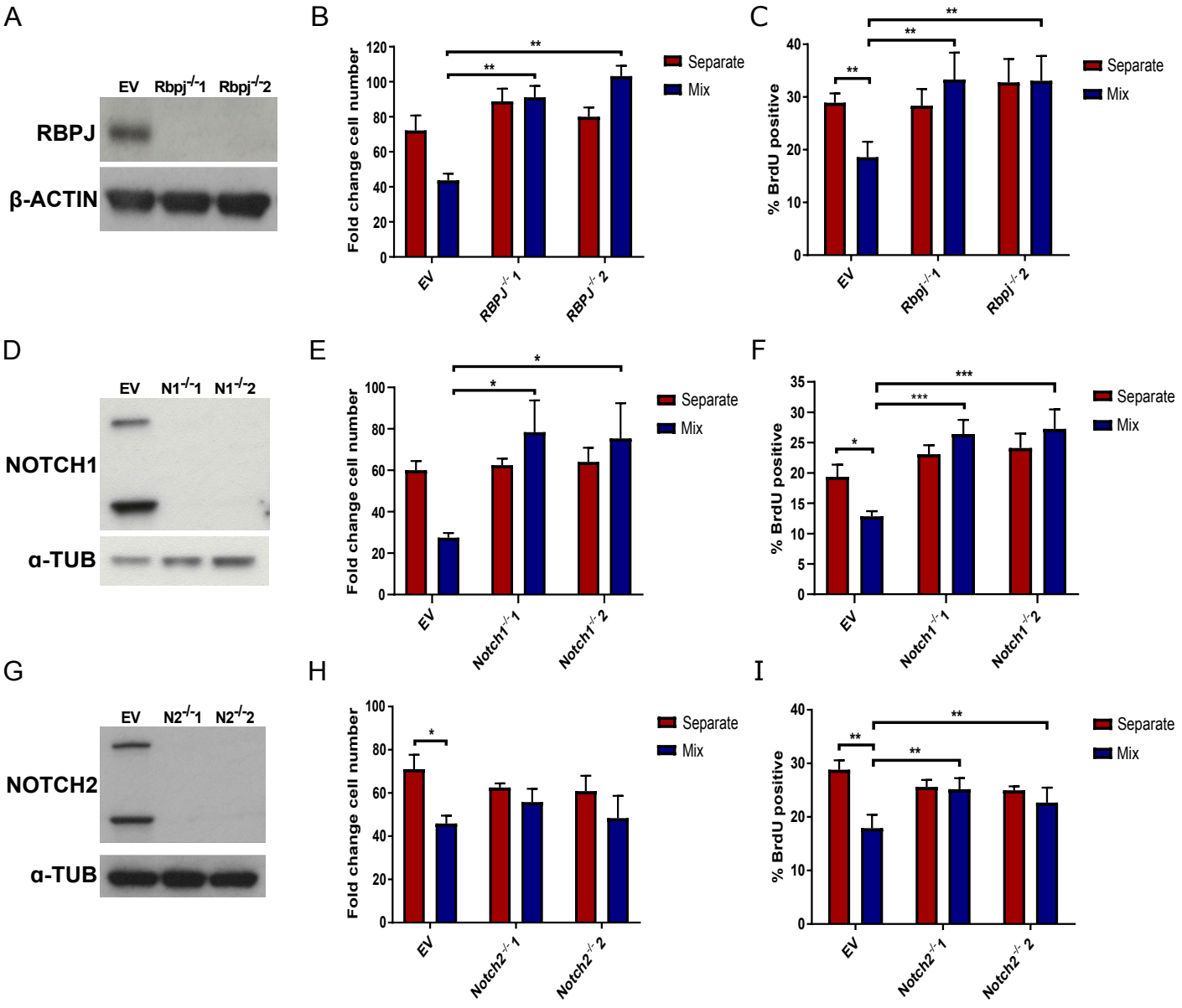
A
EV
Rbpj-/-1
Rbpj-/-2
RBPJ
β-ACTIN
B
Fold change cell number
Separate
Mix
EV
RBPJ-/-1
RBPJ-/-2
C
% BrdU positive
Separate
Mix
EV
Rbpj-/-1
Rbpj-/-2
D
EV
N1-/-1
N1-/-2
NOTCH1
α-TUB
E
Fold change cell number
Separate
Mix
EV
Notch1-/-1
Notch1-/-2
F
% BrdU positive
Separate
Mix
EV
Notch1-/-1
Notch1-/-2
G
EV
N2-/-1
N2-/-2
NOTCH2
α-TUB
H
Fold change cell number
Separate
Mix
EV
Notch2-/-1
Notch2-/-2
I
% BrdU positive
Separate
Mix
EV
Notch2-/-1
Notch2-/-2

Supplementary Figure 2

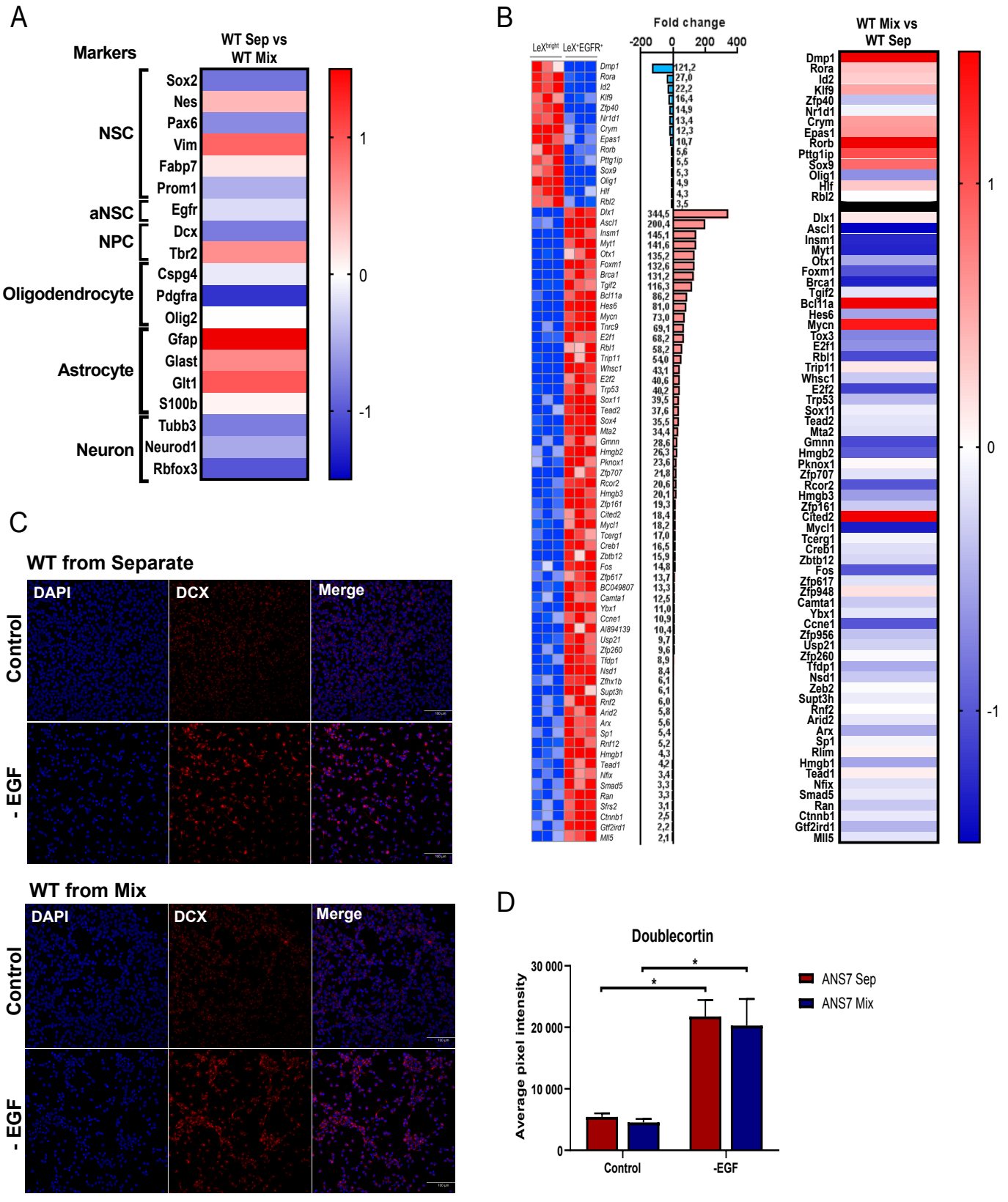

Supplementary Figure 1

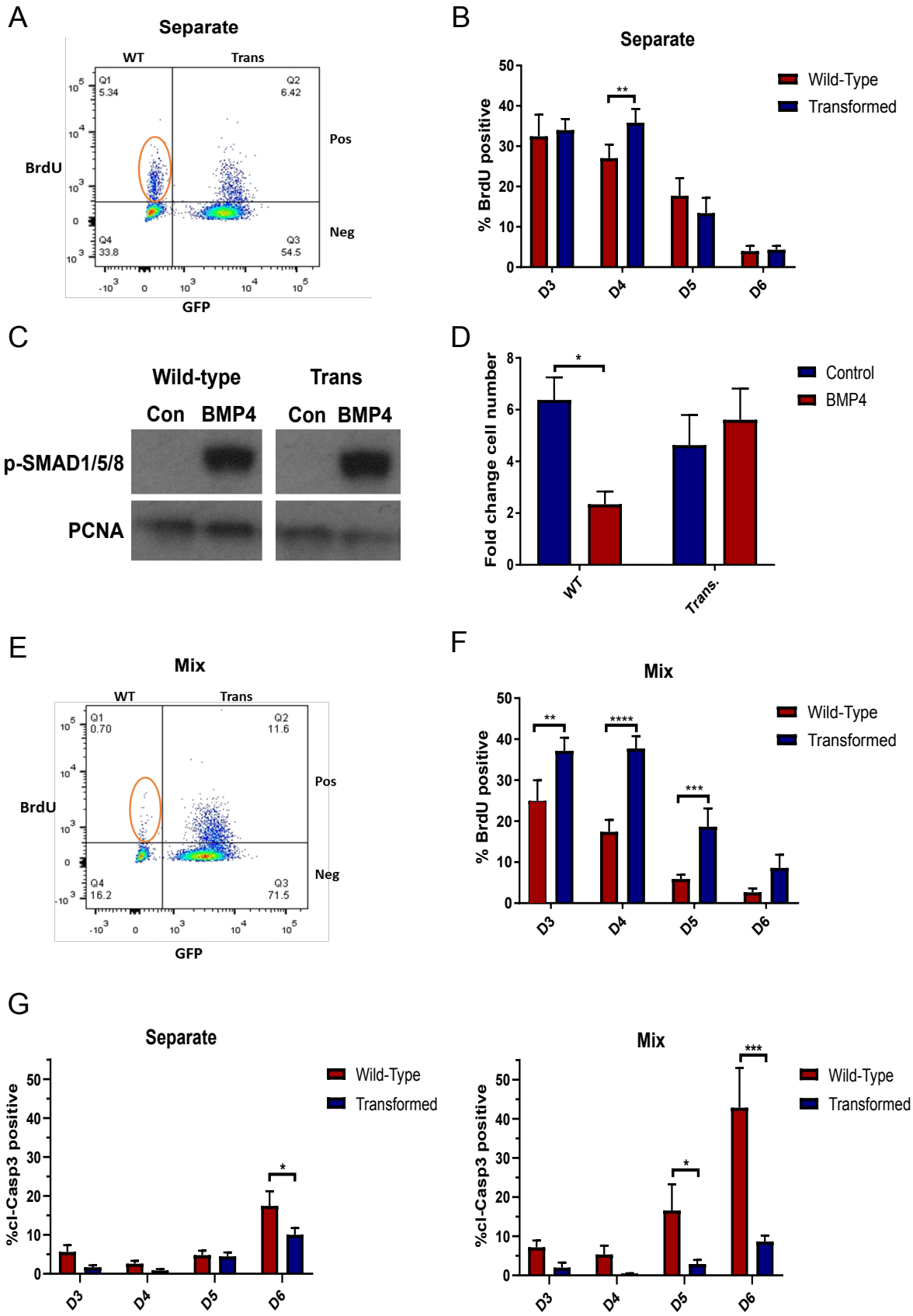

Supplementary Figure 3

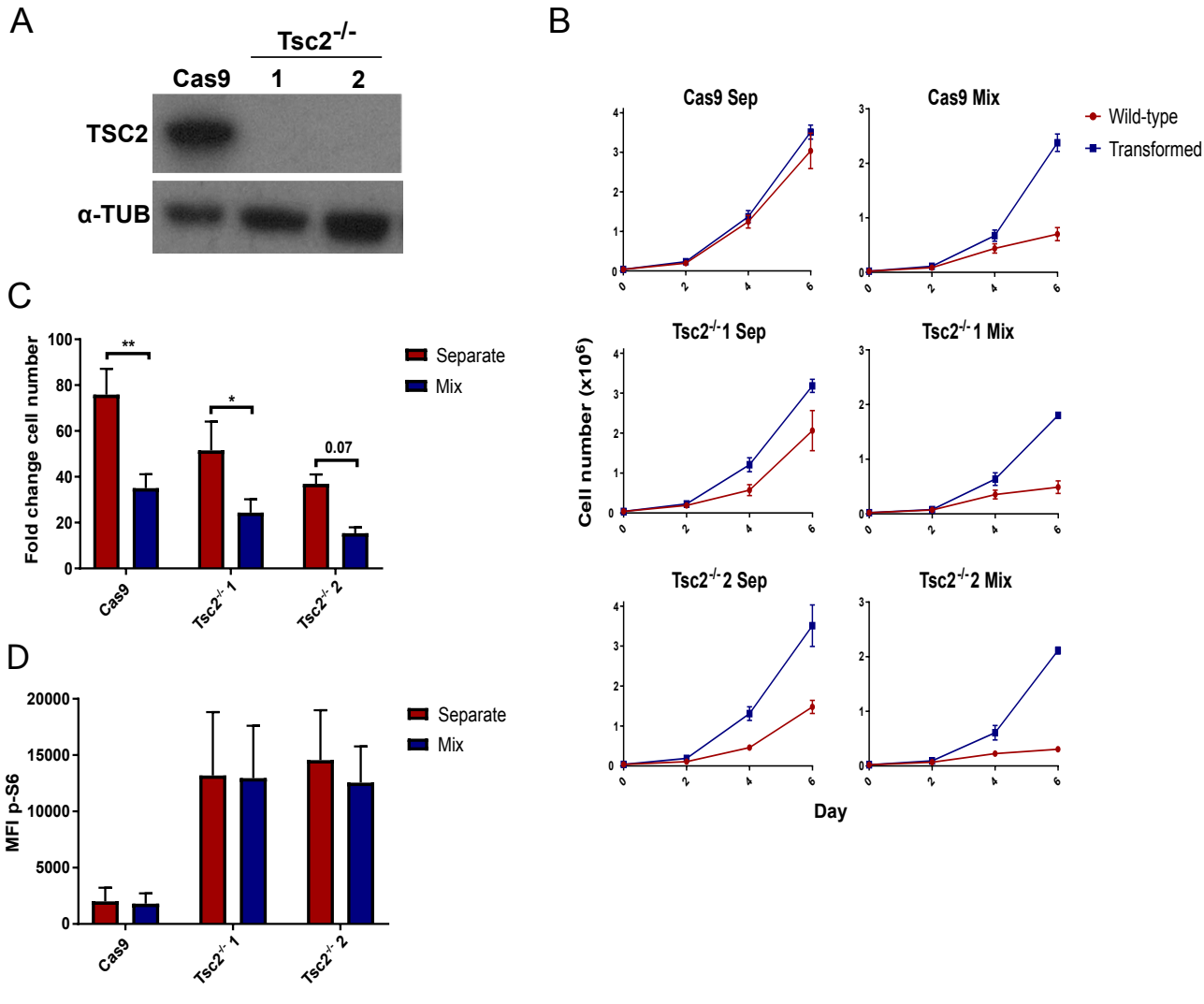

Supplementary Figure 4

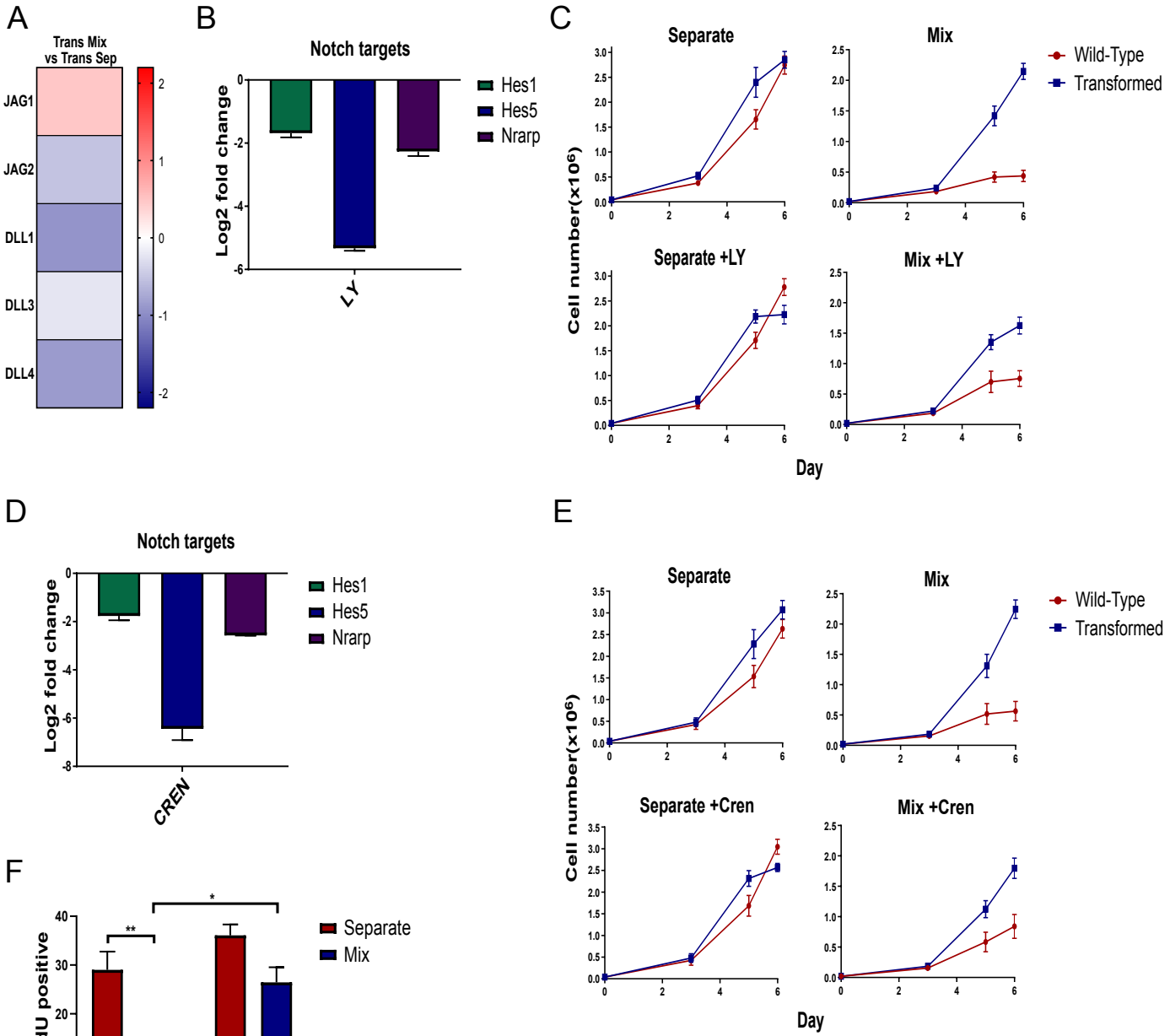

Supplementary Figure 5

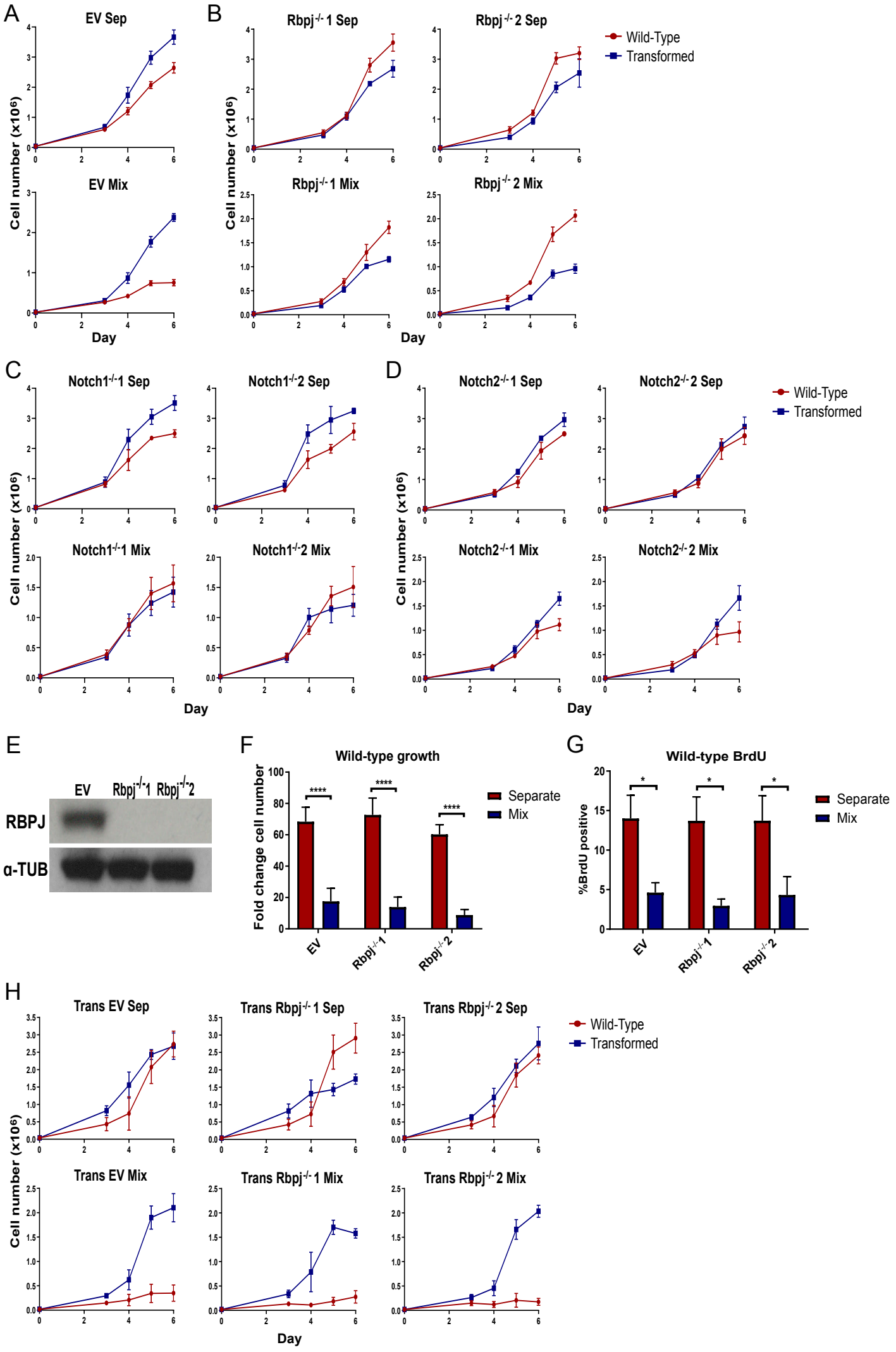

Supplementary Figure 6

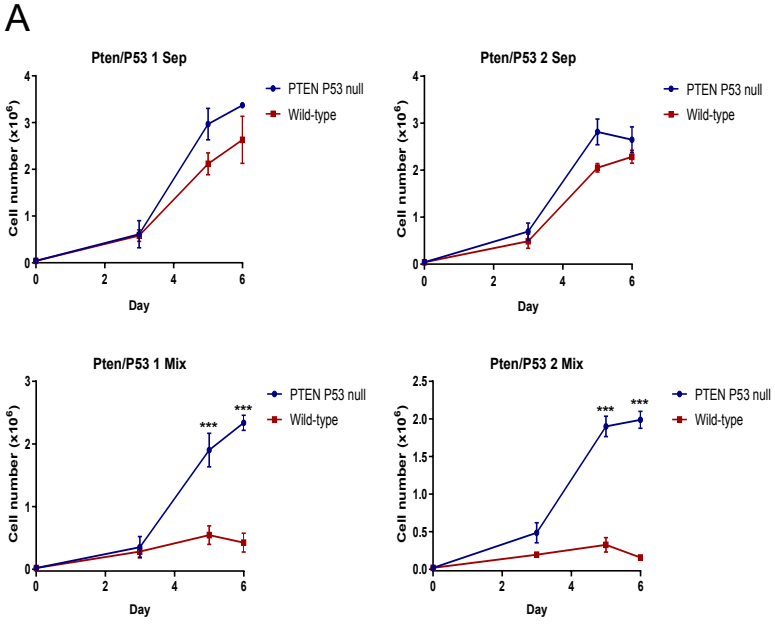

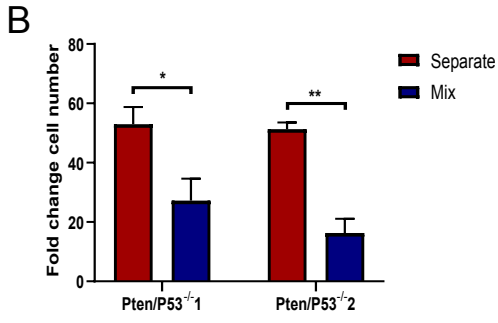

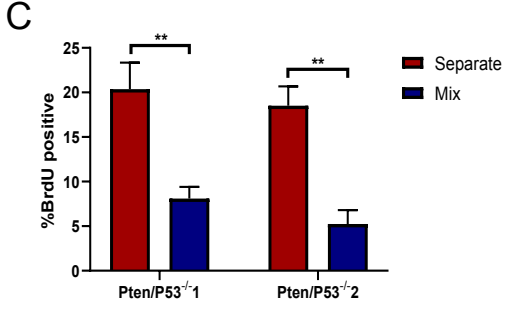

Supplemental Tables

Supplemental Table 1. Primers used in qPCR

Target gene	Forward primer	Reverse primer
Hes1	GGAAATGACTGTGAAGCACCTCC	GAAGCGGGTCACCTCGTTCATG
Hes5	GCCCGGGGTTCTATGATATT	GAGTTCGGCCTTCACAAAAG
Hes7	CATCAACCGCAGCCTAGAAGAG	CACGGCGAACTCCAGTATCTCC
Hey1	CCAACGACATCGTCCCAGGTTT	CTGCTTCTCAAAGGCACTGGGT
Hey2	TGAAGATGCTCCAGGCTACAGG	CCTTCCACTGAGCTTAGGTACC
Nrarp	CAGACAGCACTACACCAGTCAG	CCGAAAGCGGCGATGTGTAGC
β-actin	GGCACCACACCTTCTACAATG	GGGGTGTTGAAGGTCTCAAAC

Supplemental Table 2. gRNA sequences for deletion

Target gene	gRNA1	gRNA2
Rbpj	TGCAGTGGACGACGACGAGT	GTGGACGACGACGAGTCGGA
Notch1	GGCGTTCAGTGCCTACACAA	
Notch2	GTCCACCTGCATTGACCGCG	AAGTGCATCGATCACCCGAA
Tsc2	GAAGGCCGGCCTACCTCATT	GCATGGCTCTTACAGGTACA

Supplementary Figure Legends

Supplemental Figure 1

(A) Representative flow cytometry plot of BrdU staining in separately cultured NSCs at day 5. **(B)** Time-course of BrdU staining throughout the assay in separate culture. N=5, ANOVA followed by Sidak's multiple comparisons test. **(C)** Fold change cell number quantification of NSCs cultured in the presence or absence of 50ng/ml BMP4. N=4, 2-way ANOVA followed by Sidak's multiple comparisons test. **(D)** Western blot showing increased p-SMAD1/5/8 expression in NSCs treated with 50ng/ml BMP4 for 24 hours relative to control NSCs (Con). **(E)** Representative flow cytometry plot of BrdU staining in co-cultured NSCs at day 5. **(F)** Time-course of BrdU staining throughout the assay in co-culture showing reduction in BrdU incorporation in WT-NSCs. N=5, ANOVA followed by Sidak's multiple comparisons test. (**G)** Time-course of cleaved-caspase-3 expression showing increase in co-cultured WT NSCs. N=3, ANOVA followed by Sidak's multiple comparisons test.

Supplemental Figure 2

(A) Changes in gene expression of classical marker genes in the 'WT Mix vs WT Sep' comparison. GFAP $\log_2$ fold change is off the scale at 5.4. **(B)** Comparison to published transcriptional analysis of quiescent and activated NSCs. Left - Transcription factors and co-factors differentially expressed in quiescent and activated NSCs from (Morizur et al., 2018). Right – Heat map showing the expression of the genes identified by Morizur et al in the comparison of WT NSCs in separate (WT Sep) or co-culture (WT Mix). Genes enriched in quiescent NSCs were broadly upregulated in co-cultured WT NSCs, while those enriched in activated NSCs were broadly downregulated. **(C)** Immunofluorescence images and **(D)** quantification of WT-NSCs stained with Doublecortin after being grown separately or in co-culture, then sorted and re-plated in differentiation inducing conditions. N=3, 2-way ANOVA followed by Sidak's multiple comparisons test.

Supplemental Figure 3

(A) Western blot showing absence of TSC2 expression in *Tsc2*$^{-/-}$ clones. **(B)** Growth curves of transformed NSCs and *Tsc2*$^{-/-}$ or Cas9 control NSCs in separate or co-culture. *Tsc2*$^{-/-}$ clones grow more slowly than control and still show reduced growth in co-culture. N=4. **(C)** Fold change cell number quantification of growth curves. N=4, 2-way ANOVA followed by Sidak's multiple comparisons test. **(D)** Expression of p-S6 in Cas9 and *Tsc2*$^{-/-}$ clones as determined by flow cytometry. mTOR activation is increased in *Tsc2*$^{-/-}$ NSCs. N=3.

Supplemental Figure 4

(A) Heat map of RNA-seq analysis showing changes in Notch ligand gene expression in IE-NSCs. **(B)** RT-qPCR analysis of the Notch target genes, *Hes1*, *Hes5* and *Nrarp* in WT NSCs treated with 2μM LY411575. Log_2 fold change relative to control NSCs. N=3. **(C)** Growth curves of WT and transformed NSCs cultured in the standard assay with or without LY411575 addition from day 3. **(D)** RT-qPCR analysis of the Notch target genes, *Hes1*, *Hes5* and *Nrarp*

in WT NSCs treated with 1μM crenigacestat. Log_2 fold change relative to control NSCs. N=3. **(E)** Growth curves of WT and transformed NSCs cultured with or without crenigacestat addition from day 3. N=8, 2-way ANOVA followed by Sidak's multiple comparisons test. **(F)** Proportion of BrdU positive cells following a 24-hour incubation with crenigacestat. N=4, 2-way ANOVA with Sidak's multiple comparisons test. The γ-secretase inhibitor crenigacestat also increases WT NSC proliferation in co-culture.

Supplemental Figure 5

(A, B, C and D) Growth curves of control EV NSCs (A), *Rbpj*$^{-/-}$ NSCs (B), *Notch1*$^{-/-}$ NSCs (C), and *Notch2*$^{-/-}$ NSCs (D) cultured separately or in co-culture with transformed NSCs. N>4. **(E)** Western blot showing absence of RBPJ protein from *Rbpj*$^{-/-}$ transformed NSCs. **(F)** Fold change cell number of WT NSCs in separate or co-culture with EV or *Rbpj*$^{-/-}$ transformed NSCs. N=5, 2-way ANOVA followed by Sidak's multiple comparisons test. **(G)** Proportion of BrdU-positive WT NSCs in separate or co-culture with EV or *Rbpj*$^{-/-}$ transformed cells. N=3, 2-way ANOVA followed by Sidak's multiple comparisons test. **(H)** Growth curves of transformed EV and *Rbpj*$^{-/-}$ clones cultured separately or in co-culture with WT NSCs. Both *Rbpj*$^{-/-}$ clones suppress the proliferation of WT NSCs to a comparable degree to the EV control transformed cells.

Supplemental Figure 6

(A) Growth curves of control EV NSCs and *Pten*$^{-/-}$*; P53*$^{-/-}$ NSCs cultured separately or co-cultured. N=3, ANOVA followed by Sidak's multiple comparisons test. **(B)** Fold change cell number of WT NSCs in separate or co-culture with *Pten*$^{-/-}$*; P53*$^{-/-}$ NSCs. N=3, ANOVA followed by Sidak's multiple comparisons test. **(C)** Proportion of BrdU-positive WT NSCs in separate or co-culture with *Pten*$^{-/-}$*; P53*$^{-/-}$ NSCs. N=3, two-way ANOVA followed by Sidak's multiple comparisons test.

Supplemental Methods

Transwell and Fence assays

For transwell assays, 140,000 NSCs were seeded on and below PLL-coated cell culture inserts (Merck Millipore). The growth of WT NSCs seeded below WT or IE-NSCs or a 50:50 mix was evaluated over 6 days.

For Fence assays fences (Aix-Scientifics) were placed in each well of a PLL-coated 24-well plate. 100,000 NSCs were seeded in the inner ring and 400,000 in the outer ring. The fences were removed the following day and 10μM BrdU was added to the wells 48 hours after seeding for 2 hours. The fences were then replaced into the well and the cells in the inner ring were harvested and fixed in 2% formaldehyde. BrdU expression was analysed by flow cytometry as described below.

Flow cytometry immunolabelling (extended details)

Cells were fixed in 2% formaldehyde and permeabilised in ice-cold 90% methanol. Cells were incubated with the primary antibody (p-S6, cleaved-Caspase3 or BrdU, CST 1:200) for 1 hour. AlexaFluor 546 secondary antibodies (Molecular Probes) were used for detection. Controls with the primary antibody omitted were used to gate positive and negative cells. Flow cytometry was performed on an LSR-II Analyser (BD Biosciences) with FACS Diva software (BD Biosciences) and data were analysed using FlowJo software. For BrdU analysis, NSCs were incubated for two hours with 10μM BrdU prior to fixation. Before blocking, NSCs were then incubated for 45 minutes at 37°C in DNase I solution consisting of 20μl DNase I (Promega RQ1) in 250μl DNase buffer solution. The immunolabelling protocol was then followed as detailed above.

Western blot analysis

Cells were lysed directly in Laemmli buffer (50mM Tris-HCl (pH 6.8), 2% SDS, 10% glycerol in ddH_2O) and heated at 95°C for 10 minutes. Protein quantification was carried out using a BCA Protein Assay kit (Pierce) according to the manufacturer's instructions. 15-20μg denatured protein from each sample was run in XT sample buffer (BioRad) with 0.25% β-mercaptoethanol on 10% SDS-PAGE Bis-Tris gels (pre-cast BioRad). Proteins were then blotted onto PVDF membranes (Thermo Fisher Scientific). Primary antibody incubation was overnight at 4^{o}C in TBST with 5% BSA. All primary antibodies were from CST and were diluted 1:1000. Horseradish peroxidase-conjugated secondary antibodies (Abcam) diluted 1:5000 were used for detection by the addition of an enhanced chemiluminescence (ECL) substrate (Promega). Western blot quantification was performed using Fiji software (Schindelin et al. 2012).

Immunocytochemistry

Cells were fixed in 4% PFA for 10 minutes and blocked for one hour in 5% goat serum and 0.3% Triton. Primary antibodies (GFAP 1:300 Sigma, Beta-III-Tubulin 1:200 CST, DCX 1:200 Abcam) were incubated overnight at 4°C and secondary antibodies (AlexaFluor 1:600 ThermoFisher) were incubated with the coverslips for one hour. Coverslips were mounted with

Vectashield (Vector Labs) and imaged on a ZEISS LSM-780 inverted confocal microscope. Image processing and quantification of pixel intensity was performed on FIJI.

RNA Extraction and Quantitative RT-PCR

RNA was extracted with the RNeasy mini kit (Qiagen) and SuperScript III reverse transcriptase (Thermo Fisher Scientific) was used for cDNA synthesis according to manufacturer's instructions. RT-qPCR was performed using SYBR-Green Mastermix with ROX reference dye (Sigma). A list of all primer sequences can be found in Supplementary Table 1. RT-qPCR was performed on an ABI 7900HT Fast Real Time PCR machine (Applied Biosystems) and analysed on SDS Biosystem software. Relative gene expression was calculated using the ΔΔCt method normalised to β-actin expression (Livak and Schmittgen 2001).

RNA-sequencing analysis (extended details)

Sorting was performed by FACS at day 5 of the 6-day assay for 3 biological repeats. Cells were lysed and RNA extracted with the RNeasy mini kit (Qiagen). RNA samples were quantified using a Qubit fluorometer (Thermo Fisher Scientific) and the quality assessed by TapeStation electrophoresis (Agilent). mRNA was isolated using oligo dT beads. mRNA was then fragmented, converted to cDNA and ligated to Illumina adapters. Following sample indexing, the quality of cDNA libraries was also assessed by TapeStation. Sequencing was performed using the HiSeq 4000 system (Illumina). Sequencing reads were aligned using TopHat2 (Kim et al. 2013) and differential expression was analysed using the DESeq2 package (Love et al. 2014). The resulting gene sets were analysed using Ingenuity Pathway Analysis (IPA) software (Qiagen)(Kramer et al. 2014). A 'Core Analysis' was performed for each comparison on genes differentially expressed with a false discovery rate (FDR) of less than 10%.

CRISPR gene targeting of NSCs (extended details)

gRNAs for targeting of *Rbpj, Notch1*, *Notch2* and *P53*$^{-/-}$ were cloned into the pX330-U6-Chimeric_BB-CBh-hSpCas9 (PX330) expression plasmid (gift from Feng Zhang, Addgene plasmid #42230) as previously described (Ran et al. 2013). gRNAs for targeting *Tsc2* were cloned into gRNA expression plasmids (gift from George Church, Addgene plasmid #41824) (Mali et al. 2013). These were then co-transfected with an hCas9 plasmid (gift from George Church, Addgene plasmid #41815). gRNA sequences can be found in Supplemental Table 2. NSCs were transfected with plasmids by nucleofection (AMAXA 2B, Lonza) using programme A-033. 2-3x10^6 cells were resuspended in 100µl mouse neural stem cell nucleofector buffer (Lonza) with 2µg plasmid DNA. NSCs were either transfected with 2ug PX330 vector containing gRNAs targeted to *Rbpj*, *Notch1*, *Notch2* and *P53* or 0.6µg each of hCas9 and the two gRNA expression plasmids containing the *Tsc2*-targeting gRNAs. NSCs were also co-transfected with 0.125ug of Puro-pPyCAGIP vector or linear hygromycin marker (Clontech 631625) for selection. Empty vector or Cas9 only controls were also performed. Cells were recovered post-transfection with pre-warmed NSC growth media into a 10cm^2 dish. Selection with 0.25ug/ml puromycin or 250ug/ml hygromycin was performed from 48 hours post-transfection until the emergence of resistant colonies. These were then picked manually with a p20 pipette and transferred to a 48 well plate for expansion and analysis. *Pten*$^{-/-}$ NSCs

were generated as described in (Bressan et al. 2017) and then transfected with gRNAs targeting *P53* as described above.

Quantification and Statistical Analysis

Statistical analysis and data representation were performed using GraphPad Prism software. Statistical methods used are indicated in the relevant figure legends. The sample size (n) is described in the figure legends and refers to the number of independent replicate experiments performed. Adjusted p values are displayed as * $p<0.05$, ** $p<0.01$ and *** $p<0.001$.

Data availability

The raw data for the RNA-sequencing of wild-type and transformed NSCs have been deposited in the arrayexpress database under accession number E-MTAB-8580.

References

Bressan RB, Dewari PS, Kalantzaki M, Gangoso E, Matjusaitis M, Garcia-Diaz C, Blin C, Grant V, Bulstrode H, Gogolok S et al. 2017. Efficient CRISPR/Cas9-assisted gene targeting enables rapid and precise genetic manipulation of mammalian neural stem cells. *Development* **144**: 635-648.

Kim D, Pertea G, Trapnell C, Pimentel H, Kelley R, Salzberg SL. 2013. TopHat2: accurate alignment of transcriptomes in the presence of insertions, deletions and gene fusions. *Genome Biol* **14**: R36.

Kramer A, Green J, Pollard J, Jr., Tugendreich S. 2014. Causal analysis approaches in Ingenuity Pathway Analysis. *Bioinformatics* **30**: 523-530.

Livak KJ, Schmittgen TD. 2001. Analysis of relative gene expression data using real-time quantitative PCR and the 2(-Delta Delta C(T)) Method. *Methods* **25**: 402-408.

Love MI, Huber W, Anders S. 2014. Moderated estimation of fold change and dispersion for RNA-seq data with DESeq2. *Genome Biol* **15**: 550.

Mali P, Yang L, Esvelt KM, Aach J, Guell M, DiCarlo JE, Norville JE, Church GM. 2013. RNA-guided human genome engineering via Cas9. *Science* **339**: 823-826.

Ran FA, Hsu PD, Wright J, Agarwala V, Scott DA, Zhang F. 2013. Genome engineering using the CRISPR-Cas9 system. *Nat Protoc* **8**: 2281-2308.

Schindelin J, Arganda-Carreras I, Frise E, Kaynig V, Longair M, Pietzsch T, Preibisch S, Rueden C, Saalfeld S, Schmid B et al. 2012. Fiji: an open-source platform for biological-image analysis. *Nat Methods* **9**: 676-682.